International Forum on Aeroelasticity and Structural Dynamics
IFASD 2017
25-28 June 2017 Como, Italy

ON THE CONTROL OF AEROELASTIC/FLIGHT DYNAMIC INTEGRATED STABILITY OF MANEUVERING AIRCRAFT

Francesco Saltari[1], Franco Mastroddi[1], Cristina Riso[1], Guido De Matteis[1], Sara Colaianni[1]

[1]Department of Mechanical and Aerospace Engineering
Sapienza University of Rome
Via Eudossiana 18, 00185 Rome, Italy

Keywords: Flexible Aircraft, Aeroservoelasticity, Flutter Suppression, Gust Alleviation, Finite Element Method, Double Lattice Method

Abstract: This paper focuses on the application of a flexible-aircraft model for the synthesis of a robust full-state control law to suppress the body-freedom flutter instability of a flying-wing vehicle. This phenomenon is typically observed in tailless configurations as a result of the coupling between a relatively high-frequency short-period mode and a low-frequency first aeroelastic mode. Therefore, it can be captured and controlled only using a unique formulation of flight dynamics and aeroelasticity. Fully coupled equations of rigid-body motion and structural dynamics are obtained by assuming a body reference frame that verifies the practical mean-axis constraints. The equations are linearized around steady maneuvers and recast in a state-space form that simultaneously includes rigid-body, elastic, and aerodynamic state variables. The state-space model is completed with controls associated to aerodynamic surfaces and implemented for complex configurations described in terms of a finite element method structural model and a doublet lattice method aerodynamic model. Open- and closed-loop results for the stability and response of a reference flying-wing vehicle are presented and discussed to demonstrate the suitability of the integrated model to the control of flexible aircraft.

1 INTRODUCTION

The increasing flexibility in modern transport and unmanned aircraft results in low-frequency elastic modes that interact with rigid-body modes. Due to this coupling, neglecting flexibility effects when studying the vehicle flight dynamic behavior may give incorrect results on performance, stability, handling qualities, and response to pilot inputs [1, 2]. In the same way, neglecting the global aircraft motion in aeroelastic analysis may lead to inaccurate prediction of flutter margins and gust response. Appropriate models are thus necessary in order to effectively describe the coupled flight dynamic and aeroelastic behaviors of modern increasingly flexible vehicles. Such models should be also used in control synthesis. In the case of traditional configurations, the large separation in the frequency domain between rigid-body and elastic modes allows to assume rigid flight simulation models to synthesize control laws for guidance and stability augmentation [3]. For the same reason, typical aeroservoelastic problems like flutter suppression and gust alleviation were addressed without taking into account the vehicle motion as a whole [4]. However, a decoupled approach to control may be not reasonable for modern configurations, whose modes and instabilities may involve both rigid-body and elastic degrees-of-freedom. A well-known example is the body-freedom flutter [5, 6]. This instability

is typically observed in flexible flying wings as a result of the coupling between their relatively high-frequency short-period mode and the low-frequency first aeroelastic mode. In these circumstances, suppression of the body-freedom flutter can be addressed only using an integrated model of flight dynamics and aeroelasticity.

This paper investigates the validity and suitability of the fully coupled flexible-aircraft model presented in Ref. [7] for flexible aircraft control. The formulation assumes nonlinear rigid-body motion and linearized structural dynamics, and is developed using a body reference frame that satisfies the practical mean-axis constraints [1]. This approach allows to study complex configurations described in terms of a finite element method (FEM) structural model and a doublet lattice method (DLM) aerodynamic model, using data from commercial solvers for structural and aeroelastic analysis. In Ref. [7], the fully coupled equations of motion have been obtained and linearized around steady maneuvers to eventually obtain a unique state-space form for the flexible-aircraft system that simultaneously include rigid-body, elastic, and aerodynamic state variables. The state-space model has been assessed by studying the integrated stability of a recent experimental flying-wing configuration [5,6], obtaining a good agreement with reference results for the body-freedom flutter stability margin [7]. In this work, the same state-space model is augmented with additional variables associated to control surfaces and is applied for the synthesis of a full-state control law to suppress the body-freedom flutter of the flying-wing configuration studied in Ref. [7]. Since the critical mode and the most excited mode by gust loads coincide for the examined configuration, the two typical aeroservoelastic problems of flutter suppression and gust alleviation [8] can be addressed using a unique control strategy. A standard linear quadratic regulator [9] (LQR) is considered for the synthesis activities.

The paper is organized as follows. The integrated flexible-aircraft model developed in Ref. [7] is reviewed in Sec. 2, where the nonlinear equations of motion and their linearization around steady maneuvers for stability and response analysis are presented. The state-space representation of the flexible-aircraft system is described in Sec. 3. With respect to Ref. [7], the state-space model is augmented by including additional elastic state variables associated with angular rotations and rates of ailerons, rudder, and elevators, and the control surfaces are fully allowed to interact with rigid-body, elastic, and aerodynamic states. In Sec. 4 the flexible-aircraft model is used for the synthesis of a full-state control law to suppress flutter. Open- and closed-loop numerical results for the flying-wing configuration studied in Ref. [7] are presented and discussed in Sec. 4. Conclusions and future developments close the paper.

2 INTEGRATED MODEL OF FLIGHT DYNAMICS AND AEROELASTICITY

The integrated model of flight dynamics and aeroelasticity developed in Ref. [7] assumes a set of body axes that verifies the practical mean-axis constraints [1] to describe the nonlinear motion of a flexible vehicle as a whole. Structural displacements with respect to these axes are assumed small and represented in terms of a modal decomposition. Inertial coupling between rigid-body and elastic degrees-of-freedom is described in terms of a reduced set of coefficients which can be evaluated using a FEM model of the aircraft. Fully nonlinear equations of rigid-body motion and structural dynamics are obtained by the weak formulation of Cauchy's equation for a generic unrestrained continuum [10] and linearized around steady maneuvers for stability and response analysis.

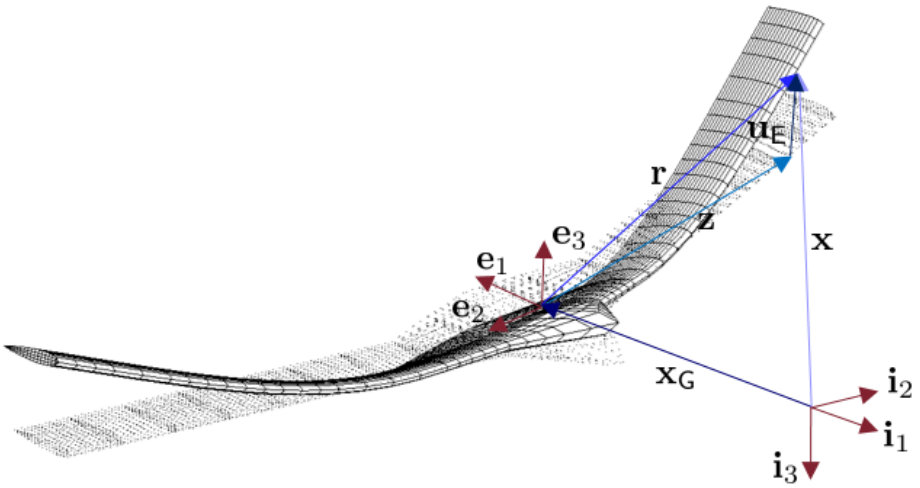

Figure 1: Reference frames to describe the motion of an unrestrained flexible vehicle.

2.1 Kinematics

The motion of an unrestrained flexible vehicle is described by assuming a set of practical mean axes (PMAs) of unit vectors $\mathbf{e}_k$ $(k = 1, 2, 3)$ as body reference frame. A set of inertial axes of unit vectors $\mathbf{i}_k$ $(k = 1, 2, 3)$ is also introduced. According to the practical mean-axis constraints [1], the PMA frame has origin at the instantaneous aircraft center of mass and it is fixed to the undeformed configuration (see Fig. 1).

The position of a generic vehicle material point P in the inertial coordinate system is given by

$$\mathbf{x} = \mathbf{x}_{\mathsf{G}} + \mathbf{z} + \mathbf{u}_{\mathsf{E}} \tag{1}$$

where $\mathbf{x}_{\mathsf{G}} = x_{\mathsf{G}}\mathbf{i}_1 + y_{\mathsf{G}}\mathbf{i}_2 + z_{\mathsf{G}}\mathbf{i}_3$ is the instantaneous position of the center of mass, $\mathbf{z} = z_1\mathbf{e}_1 + z_2\mathbf{e}_2 + z_3\mathbf{e}_3$ is the relative position of P in the PMAs in undeformed configuration, and

$$\mathbf{u}_{\mathsf{E}} = \sum_{n=1}^{\infty} q_n \boldsymbol{\phi}_n^{\mathsf{E}} \tag{2}$$

is the elastic displacement. In Eq. (2), $\boldsymbol{\phi}_n^{\mathsf{E}}$ is the nth elastic mode shape of the unconstrained structure and q_n the corresponding modal coordinate. The relative position of P with respect to the PMAs in *deformed* configuration is given by

$$\mathbf{r} := \mathbf{x} - \mathbf{x}_{\mathsf{G}} = \mathbf{z} + \mathbf{u}_{\mathsf{E}} \tag{3}$$

From Eqs. (1), (2), and (3), the absolute velocity and acceleration of P follow as

$$\mathbf{v} = \mathbf{v}_{\mathsf{G}} + \boldsymbol{\omega} \times \mathbf{r} + \mathbf{v}_{\mathsf{E}} \qquad \mathbf{a} = \dot{\mathbf{v}}_{\mathsf{G}} + \dot{\boldsymbol{\omega}} \times \mathbf{r} + \boldsymbol{\omega} \times (\boldsymbol{\omega} \times \mathbf{r}) + 2\boldsymbol{\omega} \times \mathbf{v}_{\mathsf{E}} + \mathbf{a}_{\mathsf{E}} \tag{4}$$

where $\mathbf{v}_{\mathsf{G}} = u\mathbf{e}_1 + v\mathbf{e}_2 + w\mathbf{e}_3$ is the velocity of the center of mass, $\boldsymbol{\omega} = p\mathbf{e}_1 + q\mathbf{e}_2 + r\mathbf{e}_3$ is the angular velocity of the PMA frame with respect to the inertial frame, and

$$\mathbf{v}_{\mathsf{E}} = \sum_{n=1}^{\infty} \dot{q}_n \boldsymbol{\phi}_n^{\mathsf{E}} \qquad \mathbf{a}_{\mathsf{E}} = \sum_{n=1}^{\infty} \ddot{q}_n \boldsymbol{\phi}_n^{\mathsf{E}} \tag{5}$$

are the relative velocity and acceleration due to elastic motion.

2.2 Inertial coupling

Inertial coupling between rigid-body and elastic degrees of freedom vanishes when a mean-axis body reference frame is used [11], but not in the case of a PMA frame [7, 12]. In the present model, the residual inertial coupling terms in the equations of motion are not neglected (as frequently done, see Refs. [1,2,6]). This allows to study the influence of inertial versus aerodynamic coupling effects for each application without preliminary simplifications [7]. Coupling vectors and tensors to describe inertia coupling effects are introduced below for a generic continuous structure and can be evaluated for complex configurations described by a FEM model as reported in Ref. [7].

The aircraft inertia tensor in *deformed* configuration is written as

$$\mathbf{J} = \langle \mathbf{r} \otimes \mathbf{r} \rangle = \mathbf{J}_0 + 2 \sum_{n=1}^{\infty} \mathbf{J}_n q_n + \sum_{n,m=1}^{\infty} \mathbf{J}_{nm} q_n q_m \tag{6}$$

having introduced the integral operator:

$$\langle \mathbf{a} \otimes \mathbf{b} \rangle := \iiint_{\mathcal{V}} \rho \left[(\mathbf{a} \cdot \mathbf{b}) \, \mathbf{I} - \mathbf{a} \otimes \mathbf{b} \right] \mathrm{d}\mathcal{V} \tag{7}$$

In Eq. (6), $\mathbf{J}_0$ is the inertia tensor in *undeformed* configuration, while

$$\mathbf{J}_n := \frac{1}{2} \left[\langle \mathbf{z} \otimes \boldsymbol{\phi}_n^{\mathsf{E}} \rangle + \langle \boldsymbol{\phi}_n^{\mathsf{E}} \otimes \mathbf{z} \rangle \right] \qquad \mathbf{J}_{nm} := \frac{1}{2} \left[\langle \boldsymbol{\phi}_n^{\mathsf{E}} \otimes \boldsymbol{\phi}_m^{\mathsf{E}} \rangle + \langle \boldsymbol{\phi}_m^{\mathsf{E}} \otimes \boldsymbol{\phi}_n^{\mathsf{E}} \rangle \right] \tag{8}$$

are first- and second-order coupling tensors. The sensitivity of the inertia tensor (6) on the nth modal coordinate is described by the tensor

$$\mathbf{Y}_n := \mathrm{sym} \, \langle \mathbf{r} \otimes \boldsymbol{\phi}_n^{\mathsf{E}} \rangle = \mathbf{J}_n + \sum_{m=1}^{\infty} \mathbf{J}_{nm} q_m = \frac{1}{2} \frac{\partial \mathbf{J}}{\partial q_n} \tag{9}$$

The following inertial coupling vectors are also introduced:

$$\mathbf{b}_{nm} := \iiint_{\mathcal{V}} \rho \boldsymbol{\phi}_n^{\mathsf{E}} \times \boldsymbol{\phi}_m^{\mathsf{E}} \, \mathrm{d}\mathcal{V} = -\mathbf{b}_{mn} \tag{10}$$

Using Eqs. (6), (8), and (10), the angular momentum of a generic flexible body is written as

$$\mathbf{h}_{\mathsf{G}} = \iiint_{\mathcal{V}} \rho \mathbf{r} \times (\boldsymbol{\omega} \times \mathbf{r}) \, \mathrm{d}\mathcal{V} + \iiint_{\mathcal{V}} \rho \mathbf{u}_{\mathsf{E}} \times \mathbf{v}_{\mathsf{E}} \, \mathrm{d}\mathcal{V} = \mathbf{J}\boldsymbol{\omega} + \sum_{n,m=1}^{\infty} \mathbf{b}_{nm} q_n \dot{q}_m \tag{11}$$

2.3 Nonlinear equations of motion

Having assumed a PMA body frame, the equations of motion are as follows [7]:

1. Translational equations:
$$m \frac{\mathrm{d}\mathbf{v}_{\mathsf{G}}}{\mathrm{d}t} = \mathbf{f}_{\mathsf{T}} \tag{12}$$
2. Rotational equations:
$$\frac{\mathrm{d}\mathbf{h}_{\mathsf{G}}}{\mathrm{d}t} = \mathbf{m}_{\mathsf{G}} \tag{13}$$

3. Elastic equations:

$$m_n\ddot{q}_n - \frac{\mathrm{d}\boldsymbol{\omega}}{\mathrm{d}t}\cdot\sum_{m=1}^{\infty}\mathbf{b}_{nm}q_m - \boldsymbol{\omega}\cdot\mathbf{Y}_n\boldsymbol{\omega} - 2\boldsymbol{\omega}\cdot\sum_{m=1}^{\infty}\mathbf{b}_{nm}\dot{q}_m + k_n q_n = f_n \tag{14}$$

where m is the total aircraft mass, $\mathbf{f}_{\mathsf{T}} = X\mathbf{e}_1 + Y\mathbf{e}_2 + Z\mathbf{e}_3$ and $\mathbf{m}_{\mathsf{G}} = L\mathbf{e}_1 + M\mathbf{e}_2 + N\mathbf{e}_3$ are respectively the total force and the total moment with respect to the center of mass, m_n is the nth generalized mass, k_n the nth generalized stiffness, and f_n the nth generalized force obtained by projecting loads on the mode-shape functions.

Inertial coupling between rigid-body and structural dynamics stems from the angular momentum in Eq. (13) and due to the centrifugal, Coriolis, and angular acceleration terms in Eq. (14). Aerodynamic coupling occurs through the right-hand sides of Eqs. (12), (13), and (14). Equations (12), (13), and (14) have been also obtained in Ref. [12] using a Lagrangian approach, and they reduce to the ones in Refs. [1, 2, 6] by neglecting inertial coupling effects. Further details on the derivation of Eqs. (12), (13), and (14) are found in Ref. [7].

2.4 Linearized equations of motion

The nonlinear equations in Subsec. 2.3 [Eqs. (12), (13), and (14)] are linearized for small disturbances with respect to a steady maneuver, defined by the trim translational and angular velocities $\mathbf{v}_{\mathsf{G}e}$ and $\boldsymbol{\omega}_e$ and by the corresponding linear aeroelastostatic deflection described by the modal coordinates at equilibrium q_{n_e}. Accordingly, the linearized model is as follows:

$$m\left(\Delta\dot{\mathbf{v}}_{\mathsf{G}} + \boldsymbol{\omega}_e\times\Delta\mathbf{v}_{\mathsf{G}} - \mathbf{v}_{\mathsf{G}e}\times\Delta\boldsymbol{\omega}\right) = \Delta\mathbf{f}_{\mathsf{T}} \tag{15}$$

$$\begin{aligned}\Delta\dot{\mathbf{J}}\,\boldsymbol{\omega}_e + \mathbf{J}_e\,\Delta\dot{\boldsymbol{\omega}} + \sum_{n,m=1}^{\infty}\mathbf{b}_{nm}q_{n_e}\Delta\ddot{q}_m - \mathbf{J}_e\,\boldsymbol{\omega}_e\times\Delta\boldsymbol{\omega} + \\ +\boldsymbol{\omega}_e\times\left(\Delta\mathbf{J}\,\boldsymbol{\omega}_e + \mathbf{J}_e\,\Delta\boldsymbol{\omega} + \sum_{n,m=1}^{\infty}\mathbf{b}_{nm}q_{n_e}\Delta\dot{q}_m\right) = \Delta\mathbf{m}_{\mathsf{G}}\end{aligned} \tag{16}$$

$$\begin{aligned}m_n\Delta\ddot{q}_n - \Delta\dot{\boldsymbol{\omega}}\cdot\sum_{m=1}^{\infty}\mathbf{b}_{nm}q_{m_e} - \boldsymbol{\omega}_e\cdot\Delta\mathbf{Y}_n\boldsymbol{\omega}_e + \\ -2\Delta\boldsymbol{\omega}\cdot\mathbf{Y}_{n_e}\boldsymbol{\omega}_e - 2\boldsymbol{\omega}_e\cdot\sum_{m=1}^{\infty}\mathbf{b}_{nm}\Delta\dot{q}_m + k_n\Delta q_n = \Delta f_n\end{aligned} \tag{17}$$

where

$$\begin{aligned}\mathbf{J}_e &= \mathbf{J}_0 + \sum_{n=1}^{\infty}\left(\mathbf{J}_n + \mathbf{Y}_{n_e}\right)q_{n_e} \qquad \Delta\mathbf{J} = 2\sum_{n=1}^{\infty}\mathbf{Y}_{n_e}\Delta q_n \qquad \Delta\dot{\mathbf{J}} = 2\sum_{n=1}^{\infty}\mathbf{Y}_{n_e}\Delta\dot{q}_n \\ \mathbf{Y}_{n_e} &= \mathbf{J}_n + \sum_{m=1}^{\infty}\mathbf{J}_{nm}q_{m_e} \qquad \Delta\mathbf{Y}_n = \sum_{m=1}^{\infty}\mathbf{J}_{nm}\Delta q_m\end{aligned} \tag{18}$$

Equations (15), (16), and (17) are recast in matrix form by replacing the physical perturbation vectors $\Delta\mathbf{v}_{\mathsf{G}}$, $\Delta\dot{\mathbf{v}}_{\mathsf{G}}$, $\Delta\boldsymbol{\omega}$, $\Delta\dot{\boldsymbol{\omega}}$, $\Delta\mathbf{f}_{\mathsf{T}}$, and $\Delta\mathbf{m}_{\mathsf{G}}$ by the following vectors of their components in the PMA frame:

$$\begin{aligned} \Delta\mathsf{v}_{\mathsf{G}} &= \{\Delta u,\, \Delta v,\, \Delta w\}^{\mathsf{T}} & \Delta\omega &= \{\Delta p,\, \Delta q,\, \Delta r\}^{\mathsf{T}} \\ \Delta\mathsf{f}_{\mathsf{T}} &= \{\Delta X,\, \Delta Y,\, \Delta Z\}^{\mathsf{T}} = \Delta\mathsf{f}_{\mathsf{A}} + \Delta\mathsf{f}_{\mathsf{W}} & \Delta\mathsf{m}_{\mathsf{G}} &= \{\Delta L,\, \Delta M,\, \Delta N\}^{\mathsf{T}} = \Delta\mathsf{m}_{\mathsf{A}} \end{aligned} \tag{19}$$

where $\Delta\mathsf{f}_{\mathsf{A}}$ and $\Delta\mathsf{f}_{\mathsf{W}}$ are respectively the perturbations of the aerodynamic and weight force and $\Delta\mathsf{m}_{\mathsf{A}}$ is the perturbation of the aerodynamic moment. Any other physical quantity in Eqs. (15), (16), and (17) is also represented in terms of the vector or matrix of its components in the PMA frame (for instance, the trim angular velocity $\boldsymbol{\omega}_e$ is replaced by the vector of its components ω_e). Equations (15), (16), and (17) are written in concise form as

$$\mathsf{M}_e \begin{Bmatrix} \Delta\dot{\mathsf{v}}_{\mathsf{G}} \\ \Delta\dot{\omega} \\ \Delta\ddot{\mathsf{q}} \end{Bmatrix} + \mathsf{D}_e \begin{Bmatrix} \Delta\mathsf{v}_{\mathsf{G}} \\ \Delta\omega \\ \Delta\dot{\mathsf{q}} \end{Bmatrix} + \mathsf{K}_e \begin{Bmatrix} \Delta\mathsf{x}_{\mathsf{G}}^{\mathsf{B}} \\ \Delta\theta \\ \Delta\mathsf{q} \end{Bmatrix} = \begin{Bmatrix} \Delta\mathsf{f}_{\mathsf{T}} \\ \Delta\mathsf{m}_{\mathsf{G}} \\ \Delta\mathsf{f}_{\mathsf{E}} \end{Bmatrix} \tag{20}$$

The quantities

$$\begin{aligned} \Delta\mathsf{q} &= \{\Delta q_1,\, \ldots,\, \Delta q_N\}^{\mathsf{T}} & \Delta\mathsf{f}_{\mathsf{E}} &= \{\Delta f_1,\, \ldots,\, \Delta f_N\}^{\mathsf{T}} \\ \Delta\mathsf{x}_{\mathsf{G}}^{\mathsf{B}} &= \left\{\Delta x_{\mathsf{G}}^{\mathsf{B}},\, \Delta y_{\mathsf{G}}^{\mathsf{B}},\, \Delta z_{\mathsf{G}}^{\mathsf{B}}\right\}^{\mathsf{T}} & \Delta\theta &= \{\Delta\theta_1,\, \Delta\theta_2,\, \Delta\theta_3\}^{\mathsf{T}} \end{aligned} \tag{21}$$

are respectively the perturbation vectors of the modal coordinates, generalized forces, center of mass position expressed in the PMAs, and rigid-body rotation about the PMAs. Once the generalized mass matrix $\overline{\mathsf{M}}$, the generalized stiffness matrix $\overline{\mathsf{K}}$, and the matrices

$$\begin{aligned} \mathsf{B}_e &:= \begin{bmatrix} \sum_{n=1}^{N} \mathsf{b}_{n1} q_{n_e} & \cdots & \sum_{n=1}^{N} \mathsf{b}_{nN} q_{n_e} \end{bmatrix} & \mathsf{Y}_e &:= 2 \begin{bmatrix} \mathsf{Y}_{1_e}\omega_e & \cdots & \mathsf{Y}_{N_e}\omega_e \end{bmatrix} \\ \mathsf{F}_e &:= \begin{bmatrix} \omega_e^{\mathsf{T}}\mathsf{J}_{11}\omega_e & \cdots & \omega_e^{\mathsf{T}}\mathsf{J}_{1N}\omega_e \\ \vdots & \ddots & \vdots \\ \omega_e^{\mathsf{T}}\mathsf{J}_{N1}\omega_e & \cdots & \omega_e^{\mathsf{T}}\mathsf{J}_{NN}\omega_e \end{bmatrix} & \mathsf{G}_e &:= 2 \begin{bmatrix} \omega_e^{\mathsf{T}}\mathsf{b}_{11} & \cdots & \omega_e^{\mathsf{T}}\mathsf{b}_{1N} \\ \vdots & \ddots & \vdots \\ \omega_e^{\mathsf{T}}\mathsf{b}_{N1} & \cdots & \omega_e^{\mathsf{T}}\mathsf{b}_{NN} \end{bmatrix} \end{aligned} \tag{22}$$

are introduced, the matrices in Eq. (20) are written as

$$\mathsf{M}_e = \begin{bmatrix} m\mathsf{I} & 0 & 0 \\ 0 & \mathsf{J}_e & \mathsf{B}_e \\ 0 & \mathsf{B}_e^{\mathsf{T}} & \overline{\mathsf{M}} \end{bmatrix} \quad \mathsf{D}_e = \begin{bmatrix} m\hat{\Omega}_e & -m\hat{\mathsf{V}}_{\mathsf{G}e} & 0 \\ 0 & \hat{\Omega}_e\mathsf{J}_e - \hat{\mathsf{H}}_{\mathsf{G}e} & \hat{\Omega}_e\mathsf{B}_e + \mathsf{Y}_e \\ 0 & -\mathsf{Y}_e^{\mathsf{T}} & -\mathsf{G}_e \end{bmatrix} \quad \mathsf{K}_e = \begin{bmatrix} 0 & 0 & 0 \\ 0 & 0 & \hat{\Omega}_e\mathsf{Y}_e \\ 0 & 0 & \overline{\mathsf{K}} - \mathsf{F}_e \end{bmatrix} \tag{23}$$

where $\hat{\Omega}_e$ and $\hat{\mathsf{V}}_e$ are, respectively, the skew-symmetric matrices associated with the cross product of ω_e and $\mathsf{v}_{\mathsf{G}e}$.

2.5 Small disturbance aerodynamics

Small disturbance aerodynamics is modeled via DLM, which is a potential-flow lifting surface aerodynamic model standardly used in commercial FEM aeroelastic solvers [13]. In these solvers, small disturbance unsteady aerodynamics is described in the frequency domain by the generalized aerodynamic force (GAF) matrix $\mathsf{E} := \mathsf{E}(k; M_\infty)$, where $k := \omega b/U_\infty$ is the reduced frequency, ω is the dimensional Fourier variable, b is the reference half chord, U_∞ is

the freestream velocity, and M_∞ the freestream Mach number. In a fully unsteady description, the GAF matrix has a transcendental dependency on the reduced frequency due to lag effects associated with wake dynamics. This makes the linear aeroelastic system integrodifferential, so that it cannot be directly recast in state-space form. However, a state-space representation of the aeroelastic system can be achieved by approximating the GAF matrix by means of polynomials and rational functions of k [8, 14]. Using this approach, the aerodynamic terms on the right-hand side of Eq. (20) can be represented as functions of the non-dimensional Laplace variable p as follows [7]:

$$\begin{Bmatrix} \Delta\tilde{\mathsf{f}}_{\mathsf{A}} \\ \Delta\tilde{\mathsf{m}}_{\mathsf{G}} \\ \Delta\tilde{\mathsf{f}}_{\mathsf{E}} \end{Bmatrix} = \frac{1}{2}\,\rho_\infty U_\infty\, b\,(p\bar{\mathsf{A}}_2 + \bar{\mathsf{A}}_1) \begin{Bmatrix} \Delta\tilde{\mathsf{v}}_{\mathsf{G}} \\ \Delta\tilde{\omega} \\ \Delta\tilde{\mathsf{q}} \end{Bmatrix} + q_D\,\bar{\mathsf{A}}_0 \begin{Bmatrix} \Delta\tilde{\mathsf{x}}^{\mathsf{B}}_{\mathsf{G}} \\ \Delta\tilde{\theta} \\ \Delta\tilde{\mathsf{q}} \end{Bmatrix} + q_D\,\bar{\mathsf{C}}\,(p\mathsf{I} - \bar{\mathsf{P}})^{-1}\,\bar{\mathsf{B}} \begin{Bmatrix} \Delta\tilde{\mathsf{x}}^{\mathsf{B}}_{\mathsf{G}} \\ \Delta\tilde{\theta} \\ \Delta\tilde{\mathsf{q}} \end{Bmatrix} \tag{24}$$

where Laplace transforms are denoted by a tilde, $q_D = \rho_\infty U_\infty^2/2$ is the freestream dynamic pressure, and $\bar{\mathsf{A}}_0$, $\bar{\mathsf{A}}_1$, $\bar{\mathsf{A}}_2$, $\bar{\mathsf{B}}$ and $\bar{\mathsf{C}}$ are interpolative matrices for the $(6+N)\times(6+N)$ GAF matrix data obtained from a standard FEM/DLM flutter analysis [13]. The last term in Eq. (24) approximates the wake dynamics in terms of a finite number N_a of aerodynamic states [7]

$$\Delta\tilde{\mathsf{a}} := (p\mathsf{I} - \bar{\mathsf{P}})^{-1}\,\bar{\mathsf{B}} \begin{Bmatrix} \Delta\tilde{\mathsf{x}}^{\mathsf{B}}_{\mathsf{G}} \\ \Delta\tilde{\theta} \\ \Delta\tilde{\mathsf{q}} \end{Bmatrix} \tag{25}$$

3 STATE-SPACE FLEXIBLE-AIRCRAFT MODEL

A state-space representation of the flexible-aircraft system is obtained from the linearized equations in Subsec. 2.4 [Eqs. (15), (16), and (17)] and using the small disturbance finite-state aerodynamic model in Subsec. 2.5 [Eqs. (24) and (25)]. The state-space model has order $[2(6+N)+N_a]$ and is associated to the state-space vector

$$\mathsf{y}^{\mathsf{T}} = \left\{\Delta\mathsf{v}_{\mathsf{G}}^{\mathsf{T}}, \Delta\omega^{\mathsf{T}}, \Delta\dot{\mathsf{q}}^{\mathsf{T}}, \Delta\mathsf{x}_{\mathsf{G}}^{\mathsf{T}}, \Delta\Theta^{\mathsf{T}}, \Delta\mathsf{q}^{\mathsf{T}}, \Delta\mathsf{a}^{\mathsf{T}}\right\} \tag{26}$$

where

$$\Delta\mathsf{x}_{\mathsf{G}} = \{\Delta x_{\mathsf{G}},\, \Delta y_{\mathsf{G}},\, \Delta z_{\mathsf{G}}\}^{\mathsf{T}} \qquad \Delta\Theta = \{\Delta\phi,\, \Delta\theta,\, \Delta\psi\}^{\mathsf{T}} \tag{27}$$

are the perturbation vectors of the center of mass inertial coordinates and Euler angles.

3.1 State-space matrix

The linearized equations in Subsec. 2.4 [Eqs. (15), (16), and (17)] are completed with the kinematic equations:

$$\begin{Bmatrix} \Delta\dot{\mathsf{x}}_{\mathsf{G}} \\ \Delta\dot{\Theta} \\ \Delta\dot{\mathsf{q}} \end{Bmatrix} = \mathsf{T}_1 \begin{Bmatrix} \Delta\mathsf{v}_{\mathsf{G}} \\ \Delta\omega \\ \Delta\dot{\mathsf{q}} \end{Bmatrix} = \begin{bmatrix} \mathsf{L}_e & 0 & 0 \\ 0 & \mathsf{T}_e & 0 \\ 0 & 0 & \mathsf{I} \end{bmatrix} \begin{Bmatrix} \Delta\mathsf{v}_{\mathsf{G}} \\ \Delta\omega \\ \Delta\dot{\mathsf{q}} \end{Bmatrix} \tag{28}$$

where L_e and T_e are respectively the linearized forms of the transformation matrix from the PMAs to the inertial axes and the matrix relating the Euler angles rates to the angular velocity components expressed in the PMAs. Using Eqs. (20), (24), and (25) and introducing the attitude stiffness matrix K_{W} to project the perturbation of the weight force onto the PMAs [7], the flexible-aircraft model is written in standard state-space form

$$\dot{\mathsf{y}} = \mathsf{A}\,\mathsf{y} \tag{29}$$

with state matrix [7]

$$\mathsf{A} = \begin{bmatrix} -\mathsf{M}^{-1}\mathsf{D} & -\mathsf{M}^{-1}\mathsf{K} & q_D\mathsf{M}^{-1}\bar{\mathsf{C}} \\ \mathsf{T}_1 & 0 & 0 \\ 0 & \frac{U_\infty}{b}\bar{\mathsf{B}} & \frac{U_\infty}{b}\bar{\mathsf{P}} \end{bmatrix} \tag{30}$$

where

$$\mathsf{M} := \mathsf{M}_e - \frac{1}{2}\,\rho_\infty b^2 \bar{\mathsf{A}}_2 \qquad \mathsf{D} := \mathsf{D}_e - \frac{1}{2}\,\rho_\infty U_\infty\, b\, \bar{\mathsf{A}}_1 \qquad \mathsf{K} := \mathsf{K}_e - q_D\bar{\mathsf{A}}_0 + \mathsf{K}_\mathsf{w} \tag{31}$$

The state vector elements [Eq. 26] describe the rigid-body motion of the PMA frame (12), structural displacements relative to the PMA frame ($2N$), and finite-state unsteady aerodynamics (N_a). The number of rigid-body state variables can be reduced to 9 in case aircraft flight path is out of interest for stability and response analysis [3] and the effect of the density gradient is neglected.

3.2 Gust inputs

The input matrix for gust loads is obtained by rewriting Eq. (24) as

$$\begin{Bmatrix} \Delta\tilde{\mathsf{f}}_\mathsf{A} \\ \Delta\tilde{\mathsf{m}}_\mathsf{G} \\ \Delta\tilde{\mathsf{f}}_\mathsf{E} \end{Bmatrix} = \frac{1}{2}\,\rho_\infty U_\infty\, b\,(p\bar{\mathsf{A}}_2 + \bar{\mathsf{A}}_1) \begin{Bmatrix} \Delta\tilde{\mathsf{v}}_\mathsf{G} - \tilde{\mathsf{w}} \\ \Delta\tilde{\omega} \\ \Delta\tilde{\dot{\mathsf{q}}} \end{Bmatrix} + q_D\,\bar{\mathsf{A}}_0 \begin{Bmatrix} \Delta\tilde{\mathsf{x}}^\mathsf{B}_\mathsf{G} \\ \Delta\tilde{\theta} \\ \Delta\tilde{\mathsf{q}} \end{Bmatrix} + q_D\,\bar{\mathsf{C}}\,\Delta\tilde{\mathsf{a}} \tag{32}$$

where the quasi-steady gust velocity $\tilde{\mathsf{w}}$ is assumed uniform in space over the aircraft [15]. Once Eq. (32) is developed as in Sec. 3.1, the linearized system is written as

$$\dot{\mathsf{y}} = \mathsf{A}\,\mathsf{y} + \mathsf{B}_g\,\mathsf{u}_g \tag{33}$$

where the elements of the input vector $\mathsf{u}_g^\mathsf{T} = \left\{\mathsf{w}^\mathsf{T}, \dot{\mathsf{w}}^\mathsf{T}\right\}$ are the gust velocity components and their time derivatives, and the input matrix is

$$\mathsf{B}_g = -\frac{1}{2}\,\rho_\infty U_\infty\, b \begin{bmatrix} \mathsf{M}^{-1}\bar{\mathsf{A}}_1^{(1,3)} & \frac{b}{U_\infty}\mathsf{M}^{-1}\bar{\mathsf{A}}_2^{(1,3)} \\ 0 & 0 \\ 0 & 0 \end{bmatrix} \tag{34}$$

The matrices $\bar{\mathsf{A}}_1^{(1,3)}$ and $\bar{\mathsf{A}}_2^{(1,3)}$ consist, respectively, of the first three columns of $\bar{\mathsf{A}}_1$ and $\bar{\mathsf{A}}_2$.

3.3 Control inputs

The state-space model is augmented by additional elastic state variables describing angular displacements and rates of the control surfaces. In particular, the vector of the perturbations of the generalized coordinates in Eq. (26) is rewritten as

$$\Delta\mathsf{q} = \{\Delta\delta_a, \Delta\delta_r, \Delta\delta_e, \Delta q_1, ..., \Delta q_N\}^\mathsf{T} \tag{35}$$

where $\Delta\delta_a$, $\Delta\delta_r$, and $\Delta\delta_e$ are the ailerons, rudder, and elevators angular displacements. The vector $\Delta\dot{\mathsf{q}}$ is modified accordingly by including the angular rates $\Delta\dot{\delta}_a$, $\Delta\dot{\delta}_r$, and $\Delta\dot{\delta}_e$. With this

description, the state variables associated to control surfaces are fully allowed to interact with the other elements of the state vector [Eq. (26)]. Equation (33) is rewritten as follows:

$$\dot{\mathsf{y}} = \mathsf{A}\,\mathsf{y} + \mathsf{B}_g\,\mathsf{u}_g + \mathsf{B}_c\,\mathsf{u}_c \tag{36}$$

where the components of the input vector $\mathsf{u}_c = \{\Delta m_a, \Delta m_r, \Delta m_e\}$ are the generalized forces associated to $\Delta\delta_a$, $\Delta\delta_r$, and $\Delta\delta_e$. Since the elastic modes corresponding to these variables represent rotations of ailerons, rudder, and elevators about their hinge line, the corresponding generalized forces have the physical interpretation of hinge control moments acting on these surfaces. The input matrix associated to the control moments is

$$\mathsf{B}_c = \begin{bmatrix} \mathsf{M}^{-1}\mathsf{S}_c \\ \mathsf{0} \\ \mathsf{0} \end{bmatrix} \tag{37}$$

where

$$\mathsf{S}_c = \begin{bmatrix} \mathsf{0}_{6\times 3} \\ \mathsf{I}_{3\times 3} \\ \mathsf{0}_{(N-3)\times 3} \end{bmatrix} \tag{38}$$

is a $[(9+N)\times 3]$ matrix that associates the control moments to the equations for the corresponding elastic states. Note that the number of generalized coordinates N includes those associated to global modes of the unrestrained vehicle and the additional local modes describing rotations of the control surfaces.

4 CONTROL STRATEGY

The flexible-aircraft system in Eq. (36) is controlled by applying a full-state LQR optimal control strategy [9] based on the minimization of the cost function:

$$F = \frac{1}{2}\,\mathsf{y}^{\mathsf{T}}(t_f)\mathsf{S}(t_f)\mathsf{y}(t_f) + \frac{1}{2}\int_{t=t_i}^{t=t_f} (\mathsf{y}^{\mathsf{T}}\mathsf{Q}\mathsf{y} + \mathsf{u}_c^{\mathsf{T}}\mathsf{R}\mathsf{u}_c)\,\mathrm{d}t \tag{39}$$

where R is a positive definite matrix while $\mathsf{S} = \mathsf{S}(t)$ and Q are semi-positive definite matrices. The elements of R and Q weight the state and control variables in the cost function [Eq. (39)]. The elements of the time-dependent matrix S at time t_f weight the state variables at the final time. The solution of the optimum problem in Eq. (39) with full-state feedback control law written as

$$\mathsf{u}_c = -\mathsf{K}_c\,\mathsf{y} \tag{40}$$

is given by the Riccati equation [9]. Assuming a time-invariant solution, so that $\mathsf{S} \equiv \mathsf{S}(t_f)$, solving the Riccati equation gives

$$\mathsf{u}_c = -\mathsf{R}^{-1}\mathsf{B}_c\,\mathsf{S}\,\mathsf{y} \tag{41}$$

The control law in Eq. (41) depends on the matrices Q and R weighting the state and control variables. These matrices are assumed to be diagonal and once R is assigned the matrix Q is evaluated by imposing that the quadratic forms associated to R and Q in Eq. (39) are equal for the maximum system response to a reference input u_{ref}. For instance, assuming $\mathsf{R} = \mathsf{I}$ and $\mathsf{u}_{ref} = \{1,1,1\}^{\mathsf{T}}$ gives

$$Q_{ii} = 1/\tilde{y}_{ref_i}^2 \tag{42}$$

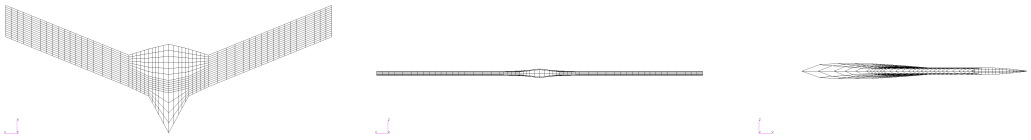

(a) Upper view (b) Front view (c) Side view

Figure 2: FEM model of the flying-wing vehicle [7].

where $\tilde{y}_{ref_i}$ is the maximum value of the ith component of the state vector due to the input u_{ref}, obtained in the frequency domain as

$$\tilde{\mathsf{y}}_{ref} = (j\omega \mathsf{I} - \mathsf{A})^{-1} \mathsf{B}\, \tilde{\mathsf{u}}_{ref} \tag{43}$$

Note that the full-state LQR optimal control strategy has been chosen for the synthesis activities in the present work due to the simplicity of its implementation for systems described by a state-space model. However, this control strategy applied to the flexible-aircraft model in Eq. (36) should require a state estimator since some of the state variables, in particular elastic and aerodynamic states, are not measurable [9]. This well-known issue is not addressed in the present work, whose purpose is to demonstrate the validity and suitability of the integrated model to flexible aircraft control. Therefore, in the following numerical studies it is assumed that all the state variables are available to implement the feedback control in Eq. (41). Development of a state estimator and use of different control strategies not based on the full state vector will be addressed in future works.

5 RESULTS AND DISCUSSION

The suitability of the state-space model in Eq. (36) to the control of flexible vehicles is assessed through the design of a control law for body-freedom flutter suppression of the reference flying wing described in Refs. [5, 6] and shown in Fig. 2. A FEM model representative of the configuration was developed in Ref. [7]. The first four elastic mode shapes of the unrestrained structure are illustrated in Fig. 3. The third mode is not shown in the figure since it describes in-plane bending. The open-loop stability and response of the configuration were studied using the present formulation [Subsec. 3.1] in Ref. [7], obtaining good agreement with reference results for the body-freedom flutter stability margin.

Once the FEM model of Ref. [7] [Fig. 2] is completed by including local modes associated to angular displacements of the control surfaces, the state-space model in Subsec. 3.3 and the control strategy in Sec. 4 are applied to suppress the body-freedom flutter instability of the configuration. Two types of analyses are carried out: 1) comparison of the open- and closed-loop root loci in steady rectilinear flight for control law designed in steady rectilinear flight at the flutter speed; and 2) comparison of the open- and closed-loop root loci in steady turn with control law designed in steady rectilinear flight and steady turn at the flutter speed.

5.1 Open-loop versus closed-loop root loci in steady rectilinear flight

The open-loop stability analysis of the aircraft in steady rectilinear flight carried out for $U_\infty = 15 \rightarrow 30$ m/s, $M_\infty = 0$, and sea level conditions showed a body-freedom flutter speed equal to $U_F^o = 20.91$ m/s [7]. The open-loop flutter speed obtained after including the local modes

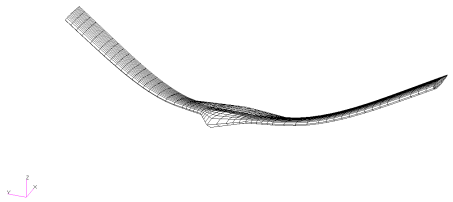

(a) $f_1 = 5.830$ Hz , $m_1 = 0.129$ kg m^2

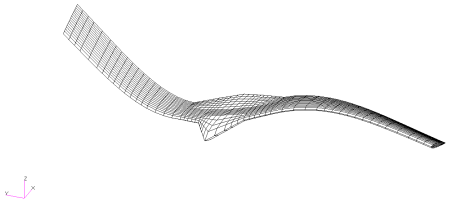

(b) $f_2 = 8.831$ Hz, $m_2 = 0.145$ kg m^2

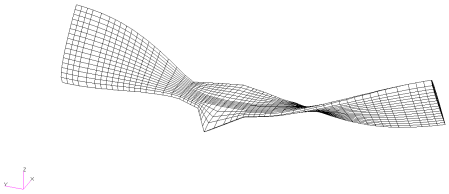

(c) $f_4 = 19.817$ Hz , $m_4 = 0.0040$ kg m^2

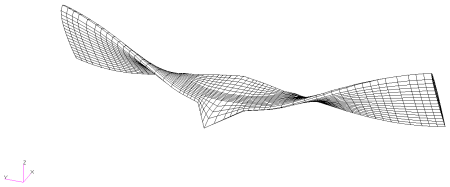

(d) $f_5 = 20.093$ Hz , $m_5 = 0.003$ kg m^2

Figure 3: Elastic mode shapes of the flying-wing FEM model [7].

associated to angular displacements of the ailerons, rudder, and elevator is equal to $U_F^o = 23.28$ m/s. This increase is due to the different aerodynamic model developed for the configuration to allow angular displacements of the panels associated to the control surfaces, which were not considered in the model of Ref. [7].

Following the design of a control law at $U_\infty = U_F^o$, according to the method recalled in Subsec. 4, the open- and closed-loop poles are compared in Fig. 4(a) to assess the control effectiveness and performance in the speed range $U_\infty = 15 \rightarrow 30$ m/s. The poles associated to the most critical modes are more clearly visible in Figs. 4(b) and 4(c). The open- and closed-loop poles at the flutter speed are emphasized by means of larger markers in the root loci. The results show that the body-freedom flutter instability is successfully suppressed and that the controller is robust with respect to variations of the flight speed although designed for a single trim condition. The flutter speed of the closed-loop system is $U_F^c = 27.60$ m/s and is associated to a classic bending-torsion instability.

5.2 Control in steady turn

The stability analysis is now carried out in steady turn at constant load factor $n_{z_e} = 2$ for the same speed range, freestream Mach number, and air density as in the previous case. The open-loop flutter speed obtained for the FEM model is $U_F^o = 23.40$ m/s and its slightly larger than the one obtained in steady rectilinear flight. In this case, the performance of controllers designed at U_F^o for the trim points in 1) steady rectilinear flight; and 2) steady turn are discussed, to evaluate the relevance of the maneuvering design point with respect to the traditional synthesis in level flight at $n_{z_e} = 1$. The two closed-loop root loci are compared in Fig. 5(a) that also shows the open-loop stability. Zooms of Fig. 5(a) are shown in Figs. 5(b) and 5(c). It is apparent that, again, the body-freedom flutter is successfully suppressed and that the controllers 1) and 2) are robust with respect to variation of the flight speed. The flutter speed of the closed-loop system is $U_F^c = 27.75$ m/s and $U_F^c = 27.85$ m/s for the design points 1) and 2), respectively. Note also

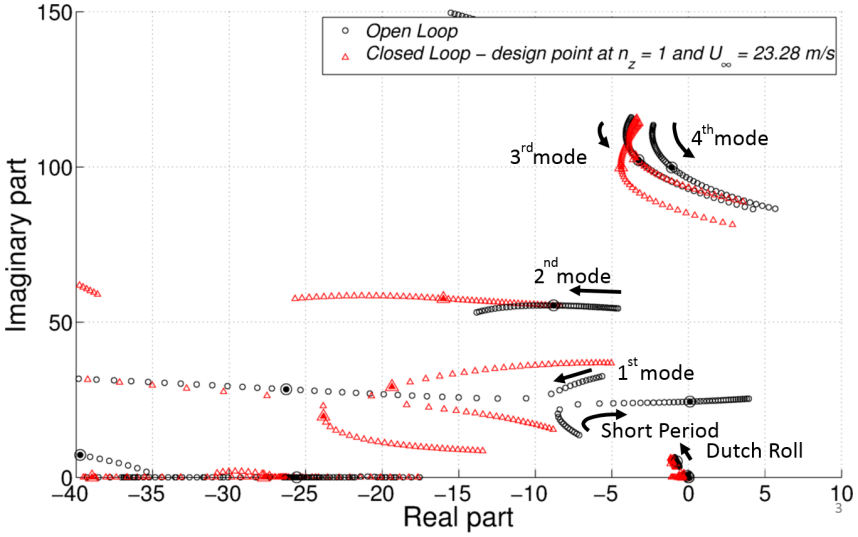

(a)

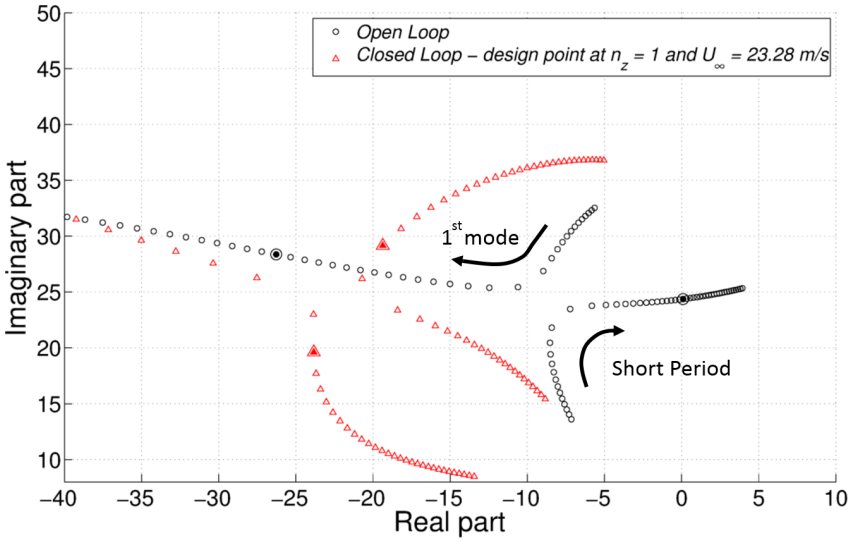

(b) Short-period and first aeroelastic mode

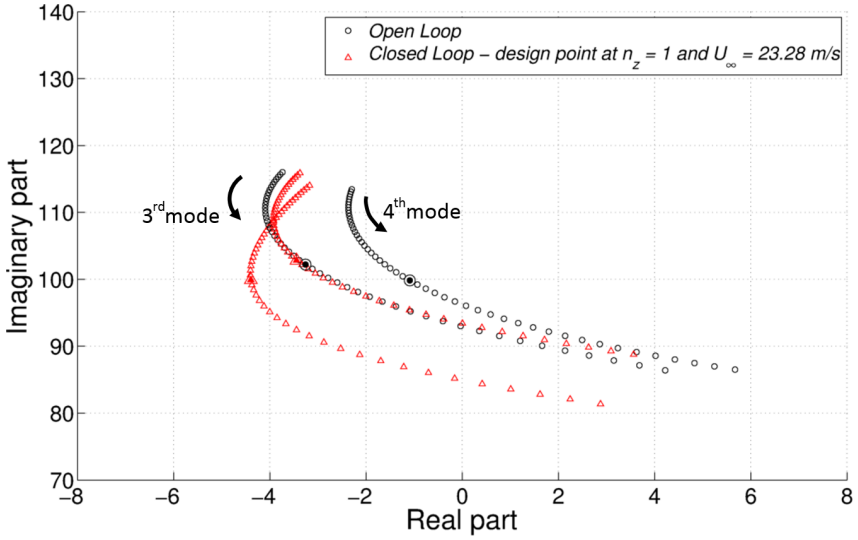

(c) Third and fourth aeroelastic modes

Figure 4: Open- and closed-loop root loci in steady rectilinear flight ($U_\infty = 15 \rightarrow 30$ m/s).

that the performance of the controllers 1) and 2) is hardly distinguishable, which is expected as Figs. 4 and 5 show that the open-loop stability is slightly influenced by the maneuvering steady state.

Since the body-freedom flutter mode is highly influenced by gust inputs [7], it is expected that the designed controller is also effective to alleviate gust loads. Therefore, as said, the two aeroservoelastic problems of flutter suppression and gust alleviation coincide for this configuration. This is demonstrated through the analysis of response to a 1-cosine gust input [15] applied to the system at the open-loop flutter speed in steady turn ($n_{z_e} = 2$). The vertical gust profile is defined in the inertial frame by the time law

$$w_g(t) = \begin{cases} 0.5\, w_{g_{max}}[1 - \cos(2\pi f_g t)] \,, & 0 < t < 1/f_g \\ 0 \,, & t \geq 1/f_g \end{cases} \tag{44}$$

with $w_{g_{max}} = 5$ m/s and $f_g = U_\infty/(25b)$ and projected in the PMA [7]. The open- and closed-loop time-histories of the center of mass vertical velocity and first modal coordinate are shown in Fig. 6, where it appears that the controller designed for flutter suppression also gives a significant alleviation of gust loads.

6 CONCLUSIONS

This paper is concerned with the application of a full-state LQR control methodology to suppress the body-freedom flutter of a representative flying-wing configuration described by an integrated flexible-aircraft model. This instability is typically observed in tailless vehicles as a result of the coupling between a relatively high-frequency short-period mode and a low-frequency first aeroelastic mode. The flexible-aircraft model considered in this paper, developed in a previous work, fully accounts for couplings between flight dynamics, structural dynamics, and unsteady aerodynamics.

For the purpose of integrated control synthesis, the state-space representation of the small-perturbation equations of motion has been augmented by additional elastic state variables associated to angular displacements and rates of the ailerons, rudder, and elevators. Control inputs in the form of hinge moments applied to the control surfaces have been also modeled. The formulation has been applied to the synthesis of control laws for suppression of the body-freedom flutter instability of a reference flying-wing vehicle.

Open- and closed-loop numerical results in steady rectilinear flight and steady turn have been discussed to demonstrate the effectiveness of the controller and its robustness with respect to flight speed and load factor. The controller has been also applied to alleviate gust loads, since due to the fact that excitation of gust disturbance mainly affects the body-freedom flutter mode it is apparent that the two typical aeroservoelastic problems of flutter suppression and gust alleviation coincide for flying-wing configurations. As a consequence, the results confirm that body-freedom flutter and gust response can be controlled by means of a single strategy.

7 REFERENCES

[1] Waszak, M. R., and Schmidt, D. K., "Flight Dynamics of Aeroelastic Vehicles", *Journal of Aircraft*, Vol. 25, No. 6, 1988, pp. 563–571.

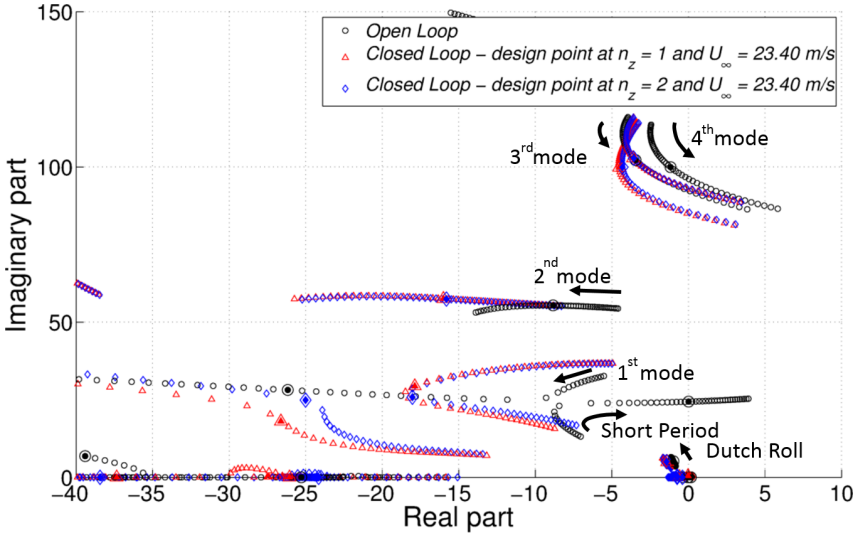

(a)

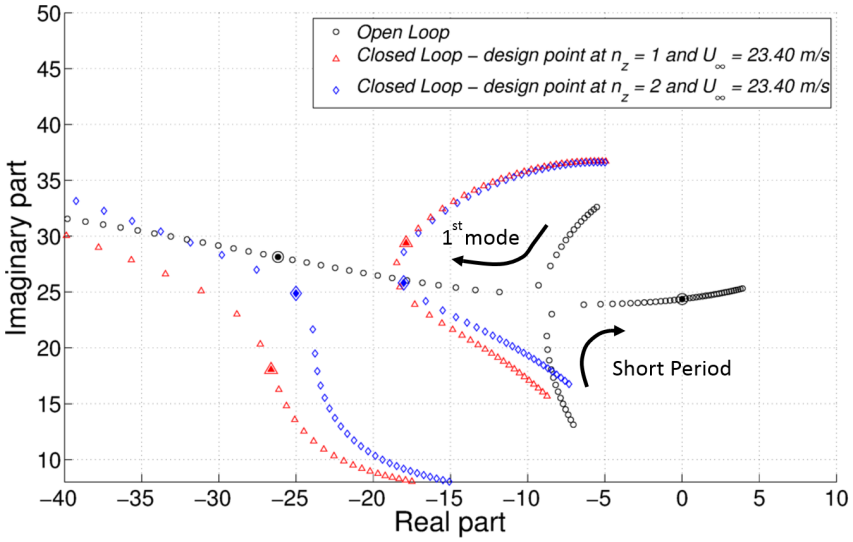

(b) Short-period and first aeroelastic mode

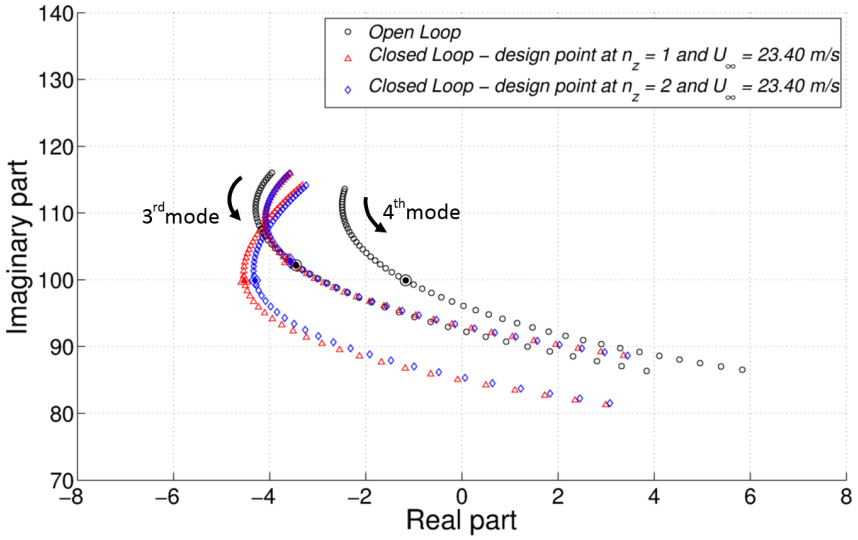

(c) Third and fourth aeroelastic modes

Figure 5: Open- and closed-loop root loci in steady turn at $n_{z_e} = 2$ ($U_\infty = 15 \rightarrow 30$ m/s).

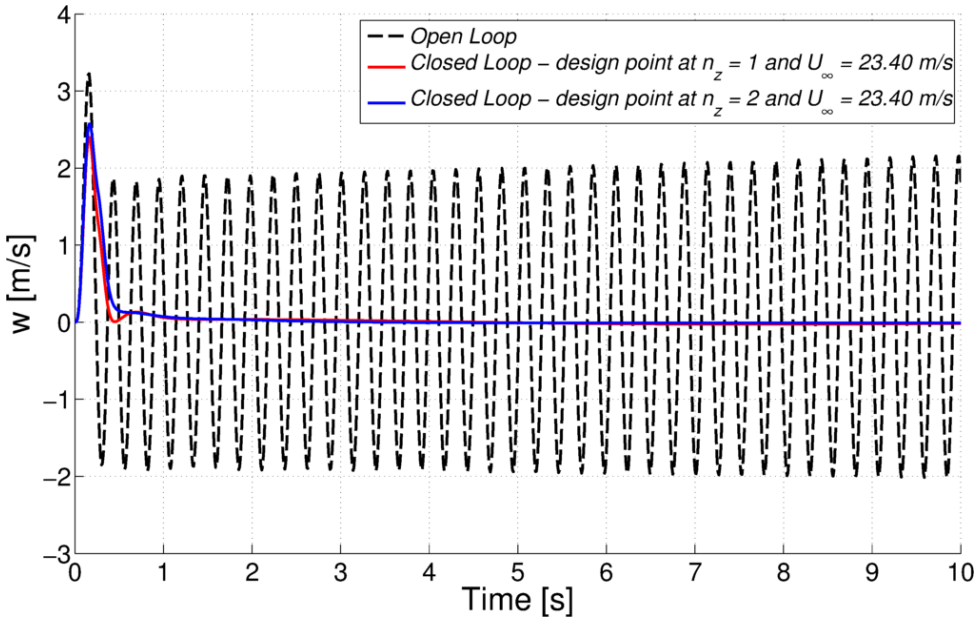

(a) Variation of the vertical velocity in PMA

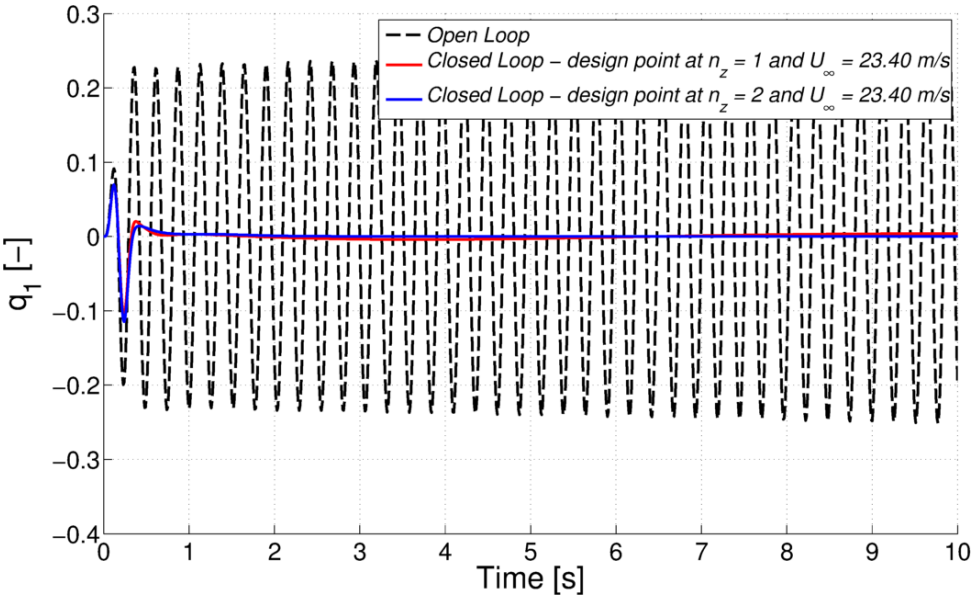

(b) Variation of the modal coordinateq_1

Figure 6: Time histories of (a) normal load factor and (b) first modal coordinate for gust load response in steady turn at sea level ($U_\infty = U_F^o = 23.40$ m/s , $n_{z_e} = 2$)

[2] Schmidt, D. K., and Raney, D. L., "Modeling and Simulation of Flexible Flight Vehicles", *Journal of Guidance, Control, and Dynamics*, Vol. 24, No. 3, 2001, pp. 539–546.

[3] Etkin, B., *Dynamics of Atmospheric Flight*, Wiley, New York, 1972.

[4] Bisplinghoff, R. L., Ashley, H., and Halfman, R.L., *Aeroelasticity*, Addison-Wesley, Reading, MA, 1955.

[5] Burnet, E.L., Atkinson, C., Beranek, J., Sibbit, B., Holm-Hansen, B., Nicolai, L., "NDOF Simulation Model for Flight Control Development with Flight Test Correlation", AIAA Paper 2010-7780, AIAA Modeling and Simulation Technologies Conference, 2 - 5 August 2010, Toronto, Ontario Canada.

[6] Schmidt, D. K. "Stability Augmentation and Active Flutter Suppression of a Flexible Flying-Wing Drone", *Journal of Guidance, Control, and Dynamics*, Vol. 39, No. 3, 2016, pp. 409–422.

[7] Saltari, F., Riso, C., De Matteis, G., Mastroddi, F., "Finite-Element Based Modeling for Flight Dynamics and Aeroelasticity of Flexible Aircraft", in press on *Journal of Aircraft*.

[8] Karpel, M., "Design for Active Flutter Suppression and Gust Alleviation Using State-Space Aeroelastic Modeling", *Journal of Aircraft*, Vol. 19, No. 3, 1982, pp. 221–227.

[9] Bryson, A. E., and Ho, Y., *Applied Optimal Control – Optimization, Estimation and Control*, Hemisphere, New York, NY, 1975.

[10] Morino, L., and Noll, R. B., "FCAP - A New Toll for the Performance and Structural Analysis for Complex Flexible Aircraft with Active Control", *Computers and Structures*, Vol. 7, 1977, pp. 275–282.

[11] Milne, R. D., "Dynamics of the Deformable Aeroplane, Parts I and II", Her Majesty's Stationery Office, Repts. and Memoranda 3345, London, Sept. 1962.

[12] Buttrill, C. S., Zeiler, T. A., and Arbuckle, P. D., "Nonlinear Simulation of a Flexible Aircraft in Maneuvering Flight", AIAA Paper 87-2501-CP, AIAA Flight Simulation Technologies Conference, August 1987, Monterey, CA.

[13] Rodden, W. P., Johnson, E. H., *MSC.Nastran Aeroelastic Analysis User's Guide*, MSC.Software Corporation, 2010.

[14] Gennaretti, M., and Mastroddi, F., "A Study of Reduced-Order Models for Gust Response Analysis of Flexible Fixed Wings", *Journal of Aircraft*, Vol. 41, No. 2, 2004, pp. 304–313.

[15] Hoblit, F.M., *Gust Loads on aircraft: Concepts and applications*, AIAA Education series, 1988.

COPYRIGHT STATEMENT